Computational Studies on Prion Proteins: Effect of Ala[117]→Val Mutation

Noriaki Okimoto,* Kazunori Yamanaka,[†] Atsushi Suenaga,[‡] Masayuki Hata,[†] and Tyuji Hoshino[†]

*Advanced Computing Center, Computational Science Division, Institute of Physical and Chemical Research (RIKEN), 2-1 Hirosawa, Wako-shi, Saitama 351-0198, Japan; [†]Graduate School of Pharmaceutical Sciences, 1-33 Yayoi-cho, Inage-ku, Chiba University, Chiba 263-8522, Japan; and [‡]Computational Research Biology Center, 2-41-6 Ohme, Koutou-ku, Tokyo 135-0064, Japan

ABSTRACT   Molecular dynamics calculations demonstrated the conformational change in the prion protein due to Ala[117]→Val mutation, which is related to Gerstmann-Sträussler-Sheinker disease, one of the familial prion diseases. Three kinds of model structures of human and mouse prion proteins were examined: (model 1) nuclear magnetic resonance structures of human prion protein HuPrP (125-228) and mouse prion protein MoPrP (124-224), each having a globular domain consisting of three α-helices and an antiparallel β-sheet; (model 2) extra peptides including Ala[117] (109-124 in HuPrP and 109-123 in MoPrP) plus the nuclear magnetic resonance structures of model 1; and (model 3) extra peptides including Val[117] (109-124 in HuPrP and 109-123 in MoPrP) plus the nuclear magnetic resonance structures of model 1. The results of molecular dynamics calculations indicated that the globular domains of models 1 and 2 were stable and that the extra peptide in model 2 tended to form a new α-helix. On the other hand, the globular domain of model 3 was unstable, and the β-sheet region increased especially in HuPrP.

INTRODUCTION

Prion diseases are manifested as familial infections or sporadic diseases, and they cause neurodegenerative disorders such as kuru, Creutzfeldt-Jacob disease, Gerstmann-Sträussler-Sheinker syndrome (GSS), and fatal familial insomnia in humans and scrapie and bovine spongiform encephalopathy (BSE) in animals (Prusiner and DeArmond, 1994). These disorders are thought to be caused by the transformation of a normal prion protein (PrP[C]) into an abnormal prion protein (PrP[SC]), which accumulates in plaques in the brain (Borchelt et al., 1990). The replication of PrP[SC] is thought to occur through interaction between PrP[SC] and PrP[C] with the assistance of a protein X acting as a chaperon (Telling et al., 1995). PrP[C] has one disulfide bridge (Fig. 1) and is anchored to the cell membrane via a glycosyl phosphatidyl inositol anchor (Stahl et al., 1987, 1992). The important point is that no chemical difference between PrP[C] and PrP[SC] has been identified (Stahl et al., 1993). However, experiments using circulator dichroism and Fourier-transform infrared analyses have shown that PrP[C] has a low β-sheet content ($\sim$3%) and is sensitive to proteases, whereas PrP[SC] has a high β-sheet content ($\sim$30%) and is protease-resistant (Pan et al., 1993; Safar et al., 1993). Recently, nuclear magnetic resonance (NMR) experiments have revealed the three-dimensional structures of mouse prion protein MoPrP (Riek et al., 1996, 1997, 1998), Syrian hamster prion protein ShPrP (Donne et al., 1997; Liu et al., 1999; James et al., 1997), bovine prion protein (García et al., 2000), and human prion protein HuPrP (Zahn et al., 2000), all of which correspond to PrP[C]. These structural data have indicated that

the N-terminal region ($\sim$125) is flexible and that the C-terminal region containing the globular domain (125-228) is rigid. The globular domain consists of three α-helices and a short antiparalell β-sheet (Fig. 2).

Most cases of human prion diseases occur spontaneously by unknown causes. However, familial prion diseases such as GSS, fatal familial insomnia, and Creutzfeldt-Jacob disease are related to distinct point mutants within the human gene of PrP[C] (PRNP) (Hsiao et al., 1989; Kretzschmar 1993). Point mutations in the PRNP gene are seen in 102, 105, 117, 145, 198, and 217 in GSS and 178, 200, and 210 in most cases of Creutzfeldt-Jacob disease. Some mutations related to GSS occur only in a few families (Tateishi et al., 1990; Hsiao et al., 1991; Mastrianni et al., 1995), e.g., P102L mutation was detected in more than 30 families, whereas Ala[117]→Val mutation was detected in only three families (Tranchant et al., 1997). It is interesting that Ala[117]→Val mutation requires two changes in the genetic code to generate an amino acid change. It is known that Ala[117]→Val mutation is coupled with Val[129], which is Met/Val heterozygous at codon 129 (Tranchant et al., 1997). Other experiments on peptides with Ala[117]→Val mutation have shown that the β-sheet region tended to increase (Brown 2000). In the current work, focusing on the Ala[117]→Val mutation, we tried to elucidate the correlation between Ala[117]→Val mutation and prion protein (PrP) structure using molecular dynamics (MD) and quantum chemical calculations.

METHODS

Molecular dynamics simulations

Construction of initial structure

MD simulations were performed on three kinds of model structures of HuPrP and MoPrP. These three model structures were constructed as follows.

Model 1 was derived from the NMR structures of HuPrP (125-228) (PDB code (Berman et al., 2000): 1QM2 (Zahn et al., 2000)) and MoPrP

	109	110
Hu	M	K
Mo	F	F

111	112	113	114	115	116	117	118	119	120	121	122	123	124	125	126	127	128	129	130
H	M	A	G	A	A	A	A	G	A	V	V	G	G	L	G	G	Y	M	L
H	V	A	G	A	A	A	A	G	A	V	V	G	G	L	G	G	Y	M	L
													-				B	B	B
													-				B	B	B
																		S1	

131	132	133	134	135	136	137	138	139	140	141	142	143	144	145	146	147	148	149	150
G	S	A	M	S	R	P	I	I	H	F	G	S	D	Y	E	D	R	Y	Y
G	S	A	M	S	R	P	M	I	H	F	G	N	D	W	E	D	R	Y	Y
B													A	A	A	A	A	A	A
B													A	A	A	A	A	A	A
					Strand1												H1		

151	152	153	154	155	156	157	158	159	160	161	162	163	164	165	166	167	168	169	170
R	E	N	M	H	R	Y	P	N	Q	V	Y	Y	R	P	M	D	E	Y	S
R	E	N	M	Y	R	Y	P	N	Q	V	Y	Y	R	P	V	D	Q	Y	S
A	A	A	A							B	B	B	B						
A	A	A								B	B	B	B						
				Strand2							S2					Strand3			

171	172	173	174	175	176	177	178	179	180	181	182	183	184	185	186	187	188	189	190
N	Q	N	N	F	V	H	D	C*	V	N	I	T	I	K	Q	H	T	V	T
N	Q	N	N	F	V	H	D	C*	V	N	I	T	I	K	Q	H	T	V	T
		A	A	A	A	A	A	A	A	A	A	A	A	A	A	A	A	A	A
	A	A	A	A	A	A	A	A	A	A	A	A	A	A	A	A	A	A	A
										H2									

191	192	193	194	195	196	197	198	199	200	201	202	203	204	205	206	207	208	209	210
T	T	T	K	G	E	N	F	T	E	T	D	V	K	M	M	E	R	V	V
T	T	T	K	G	E	N	F	T	E	T	D	V	K	M	M	E	R	V	V
A	A	A	A						A	A	A	A	A	A	A	A	A	A	A
A	A	A	A						A	A	A	A	A	A	A	A	A	A	A
			Strand4																

211	212	213	214	215	216	217	218	219	220	221	222	223	224	225	226	227	228	229	230
E	Q	M	C*	I	T	Q	Y	E	R	E	S	Q	A	Y	Y	Q	R		
E	Q	M	C*	V	T	Q	Y	Q	K	E	S	Q	A	Y	Y	Q	R		
A	A	A	A	A	A	A	A	A	A	A	A	A	A	A	A	A	A	-	
A	A	A	A	A	A	A	A	A	A	A	A	A	A	-					
			H3																

FIGURE 1 Primary structures of HuPrP and MoPrP used in this study. NMR structures of HuPrP and MoPrP consist of residues 125-228 and 124-224 (indicated by − to −). PrP has one disulfide bridge between residues 179 and 214 (indicated *asterisks*) and is anchored to the cell membrane via a glycosyl phosphatidyl inositol anchor. This figure includes information on the secondary structure elements (*gray regions* denote α-helices (H1, H2, and H3) and β-sheet (S1 and S2)). Four regions (between S1 and H1, H1 and S2, S2 and H2, and H2 and H3) were named strands 1 to 4. Amino acid numbering is according to HuPrP.

(124-224) (PDB code (Berman et al., 2000): 1AG2 (Riek et al., 1996)). The model includes a globular domain, structured part. We called this model a "control structure." Model 2 was constructed by adding an extra peptide chain containing Ala[117] (109-124 in HuPrP and 109-123 in MoPrP) to each of the NMR structures. We called this model a "wild structure." Model 3 was constructed by adding an extra peptide chain containing Val[117] (109-124 in HuPrP and 109-123 in MoPrP) to each of the NMR structures. We called this model a "mutant structure." The extra peptide chains of the wild and mutant structures were made by quantum chemical calculation (modified neglect of diatomic overlap parametric method 3

FIGURE 2 Molecular mechanics potential energy-minimized structures of the NMR-determined parts of HuPrP (*a*) and MoPrP (*b*).
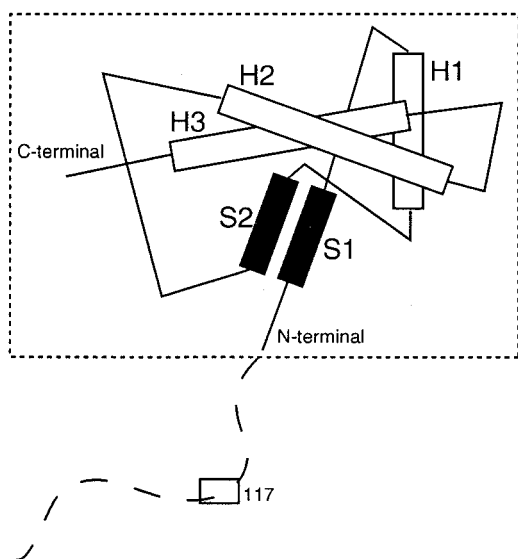
(a)

(b)
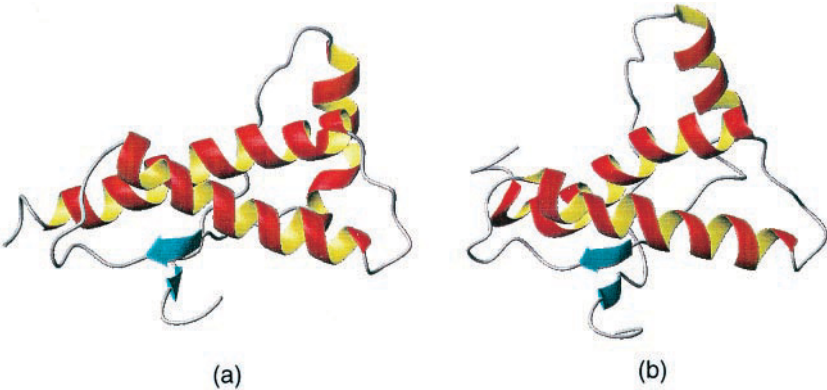
FIGURE 3 Construction of model structures. The control structure (NMR-determined structure) is enclosed by a rectangle. The control structure containing the globular domain consists of three α-helices (H1, H2, and H3) and a short β-sheet (S1 and S2). In the wild and mutant structures, the extra peptide chain is indicated by a broken line.

approximation) to obtain a locally energy-minimized structure without any definite formation like an α-helix or β-sheet, because the N-terminal region (~125) of PrP was unstructured (Fig. 3).

Details of computation

Molecular mechanics potential energy minimizations and MD simulations were carried out using the program package AMBER5.0 (Case et al., 1997). The all-atom force field of Cornell et al. (1995) was used in all MD simulations. The system was solvated with TIP3P water molecules (Jorgensen et al., 1983) generated in a rectangular box. The number of solvent water molecules in each system is shown in Table 1. A periodic boundary condition was applied, and the pressure was kept constant in the system. The temperature was kept constant by using Berendsen algorithm (Berendsen et al., 1984) with a coupling time of 0.2 ps. Only bond lengths involving hydrogen atoms are constrained using the SHAKE method (Ryckaert et al., 1977). The nonbonded interactions were calculated by a cutoff method. The distance of the cutoff was 14 Å. The integration time step of the MD simulations was 1 fs.

The procedure used in our simulations is as follows. First, potential energy minimizations were performed on each of the initial systems. In case of wild and mutant structures, after minimizations of only extra peptide chains and solvent water molecules, the potential energies of the respective whole systems were minimized. Next, MD simulations were performed on the energy-minimized systems. In the system of control structures, after 10-ps MD simulation at 600 K only for solvent water molecules, the temperatures of the whole systems were gradually increased

by heating to 300 K for 70 ps and then kept at 300 K for the next 2 ns. In the systems of wild and mutant structures, after 20-ps MD simulations at 600 K only for the extra peptide chains and solvent water molecules (to remove the arbitrariness for the extra peptide chains of the N-terminal region), the whole system was gradually heated to 300 K for 70 ps, and then the temperatures were kept at 300 K for the next 2 ns. The trajectories at 300 K for 2 ns were considered to be the most probable structure under physiological conditions and were analyzed in detail.

Secondary structures were analyzed using PROCHECK (Laskowski et al., 1993), and images of simulated prion proteins were generated using MOLMOL (Koradi et al., 1996).

Quantum chemical calculations

The models for quantum chemical calculations were constructed by extracting the extra peptide chains (109-124) from molecular mechanics potential energy-minimized structures of wild and mutant structures of HuPrP, and then their C termini were capped with $-NHCH_3$. Molecular-orbital calculations with modified neglect of diatomic overlap parametric method 3 approximation (Stewart, 1989a,b) were carried out to estimate the electronic structure. The computational program used is MOPAC version 6.0 (Stewart and Frank, 1990).

RESULTS

RMSD and residue-based RMSD

Fig. 4(*a* and *b*) show root mean square deviations (RMSDs) of whole parts (109-228) and globular domains (125-228) of HuPrP models. The RMSD of the control structure was kept at 3 Å for 2 ns, which indicated that the globular domain was considerably stable. The RMSDs of whole parts of wild and mutant structures increased rapidly within 200 ps and then fluctuated in the region of 6 to 7 Å. In addition, the RMSD of the globular domain of the wild structure, as well as that of the control structure, was maintained at approximately 3 Å for 2 ns, whereas the RMSD of the globular domain of the mutant structure gradually increased and fluctuated in the region of 5 to 6 Å after 1 ns. Fig. 5 *a* shows the residue-based RMSDs of HuPrP models. In the control structure, the residue-based RMSD values were small on the whole despite some deviation in the N-terminal region (125-127). In the globular domain of the wild structure, although the values at H1 and the C-terminal side of H3 were somewhat large, the values in other parts were as small as those in the control structure. The extra peptide chain (109-124) of the N-terminal region had very large values (over 10 Å). In the mutant structure, the values at a strand between S1 and H1 (strand 1), H1, the C-terminal side of H2, and the C-terminal side of H3 were clearly larger. We found that the extra peptide chain of the N-terminal region also had values larger than 10 Å, as was seen in the wild structure. Analysis of the residue-based RMSDs indicated that all structures (control, wild, and mutant) have common characteristics of small values of S1 and S2.

TABLE 1 Solvent water molecules in each system

	HuPrP	MoPrP
Control	9025	8204
Wild	12,336	10,761
Mutant	12,426	10,752

FIGURE 4 Root-mean-square deviations of the main chain atoms ((a) RMSD of the whole part of HuPrP, (b) RMSD of the globular domain of HuPrP, (c) RMSD of the whole part of MoPrP, and (d) RMSD of the globular domain of MoPrP). Black, blue, and red lines indicate RMSDs of the control, wild, and mutant structures, respectively. With regard to the initial states of MD simulations, the structures of these globular domains were very similar. The ordinate is RMSD (Å), and the abscissa is time (ps).
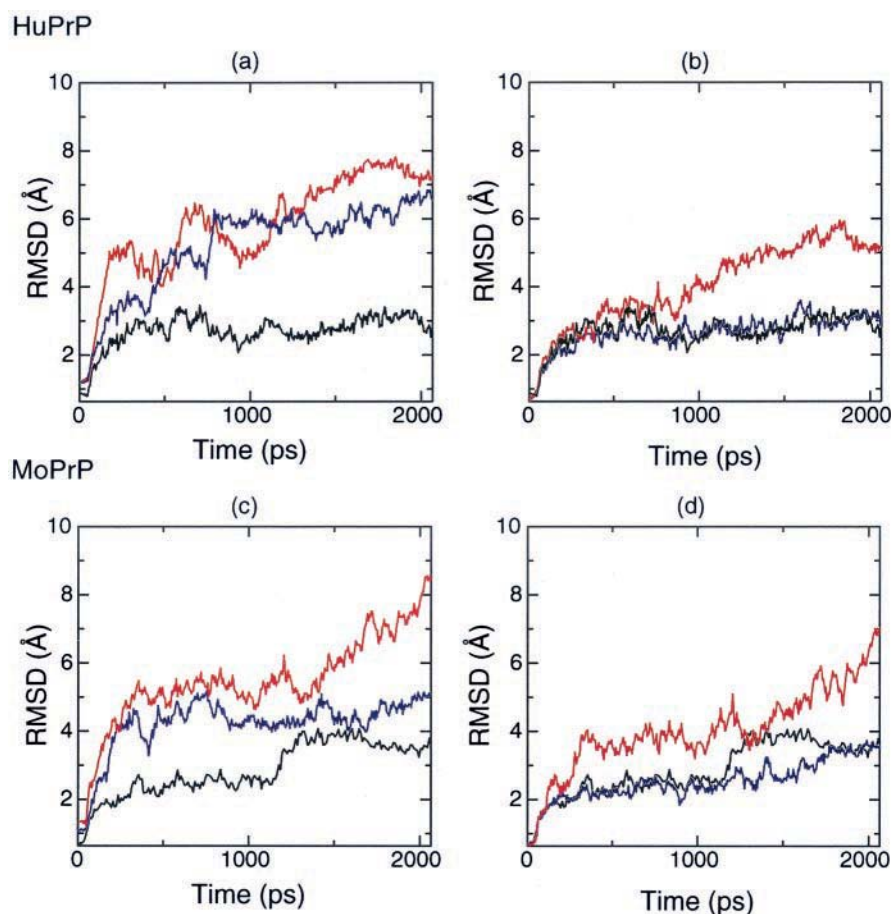
Fig. 4 (c and d) show RMSDs of whole parts (109-224) and globular domains (124-224) of MoPrP models. The RMSD of the control structure remained at ~3 Å for 2 ns, indicating significant stability of the structure. The RMSDs of whole parts of the wild and mutant structures increased rapidly within 200 ps and then fluctuated in the range of 4 to 5 Å and 5 to 8 Å, respectively. Observation of RMSDs in the globular domain revealed that the RMSD of the wild structure was similar to that of the control structure and that its globular domain was completely stabilized. On the other
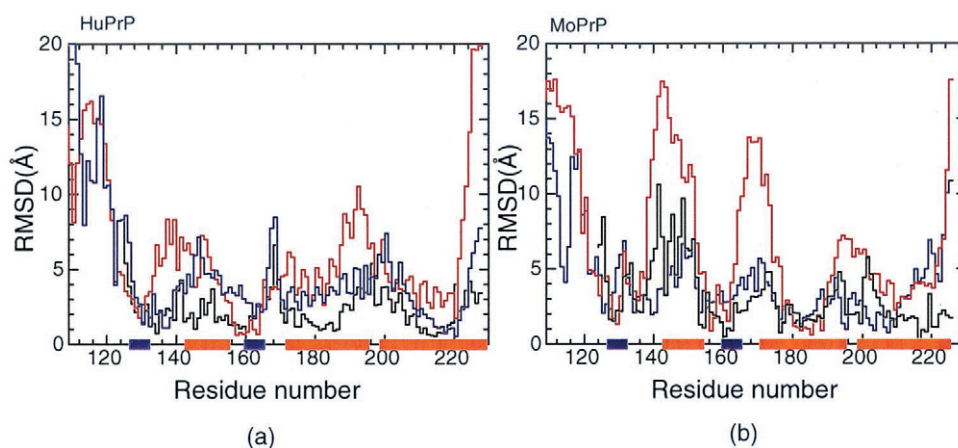
FIGURE 5 Residue-based root-mean-square deviations (residue-based RMSDs) of the main chain atoms ((a) residue-based RMSD of HuPrP and (b) residue-based RMSD of MoPrP). RMSDs of the control, wild, and mutant structures are shown by black, blue, and red lines, respectively. The α-helices and β-sheet in Fig. 1 are shown as orange and blue bonds on the abscissa, respectively. The ordinate is RMSD (Å), and the abscissa is residue number.
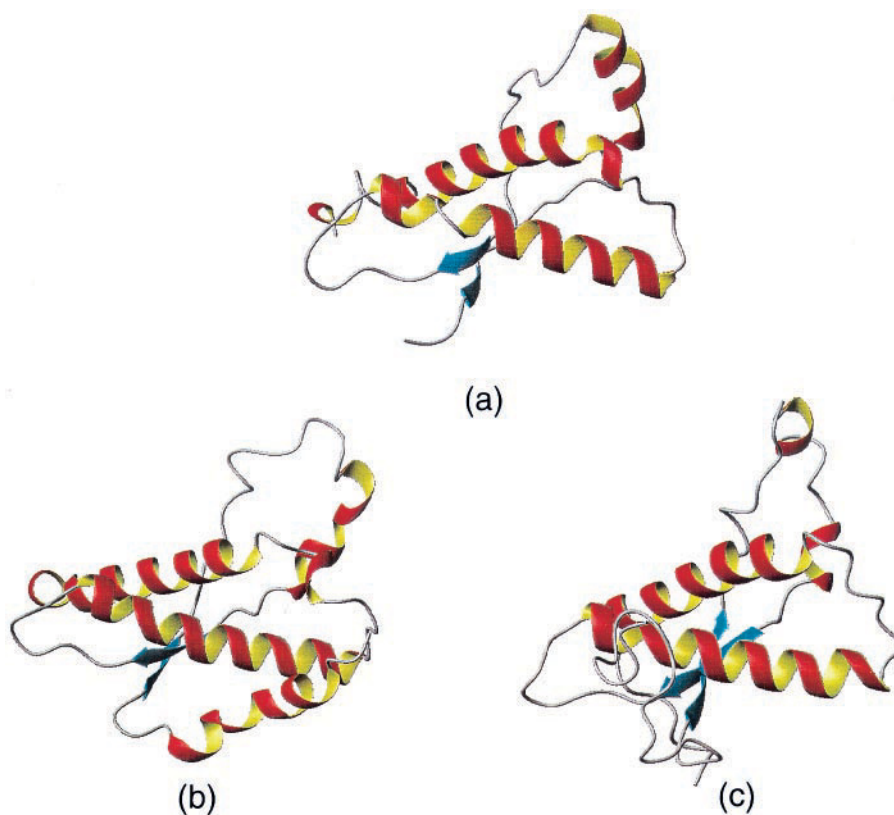
FIGURE 6 Average structures of HuPrP models ((a) control structure, (b) wild structure, and (c) mutant structure). These structures were obtained from the final 1-ns MD simulations.

hand, the RMSD of the mutant structure changed from 4 to 7 Å; thus, its conformation was very different from the control structure. The residue-based RMSDs of MoPrP models (Fig. 5 b) indicated that the values of the control structure were small on the whole despite some deviation in the N-terminal region (125-127) and H1. In the globular domain of the wild structure, although the C-terminal side of H3 had large values, the values of other parts were as small as those of the control structure. The extra peptide chain (109-123) of the N-terminal region had large values (10–14 Å). In the mutant structure, the values at H1, a strand between S2 and H2 (strand 3), a strand between H2 and H3 (strand 4), and the C-terminal side of H3 were far larger than those in the control and wild structures. The extra peptide chain of the N-terminal region also had very large values (10–18 Å) as was seen in the wild structure of MoPrP. The values of S1 and S2 were small in all structures (control, wild, and mutant), as consistently seen in those of HuPrP models.

These data revealed that the large RMSD of the whole part of the wild structure arose not from structural change in the globular domain but from structural change in the extra peptide chain of the N-terminal region. On the other hand, the large RMSD of the whole part of the mutant structure was due not only to the structural change in the extra peptide chain of the N-terminal region but also to the dramatic structural change in the globular domain.

MD simulation structures

HuPrP

The average control structure is shown in Fig. 6 a. This figure indicates that the globular domain containing three α-helices and a short antiparallel β-sheet is stably maintained. The secondary structures of the control structure were similar to those of the NMR structure of HuPrP, although the α-helix at the C-terminal side of H3 was slightly transformed into a 3_{10}-helix after 1.5 ns (Fig. 7 a). Moreover, the contact map (Fig. 8 a) indicated that the final structure, the MD simulation structure at 2 ns, matched the initial structure of MD simulation. Accordingly, the control structure was concluded to be stably maintained for 2 ns of MD simulation.

A noticeable feature of the average wild structure was that the extra peptide chain in the N-terminal region, which was a random strand at initial state of MD simulation, formed a new α-helix (H0) (Fig. 6 b). This extra peptide chain began to form α- and 3_{10}-helices at ~700 ps, and then the new α-helix, H0, was almost completed within the extra peptide chain at 2 ns.

This observation was supported by the finding that the sum of α- and 3_{10}-helix contents in the globular domain was less than those of the whole structure by ~10 amino acid residues (Table 2).
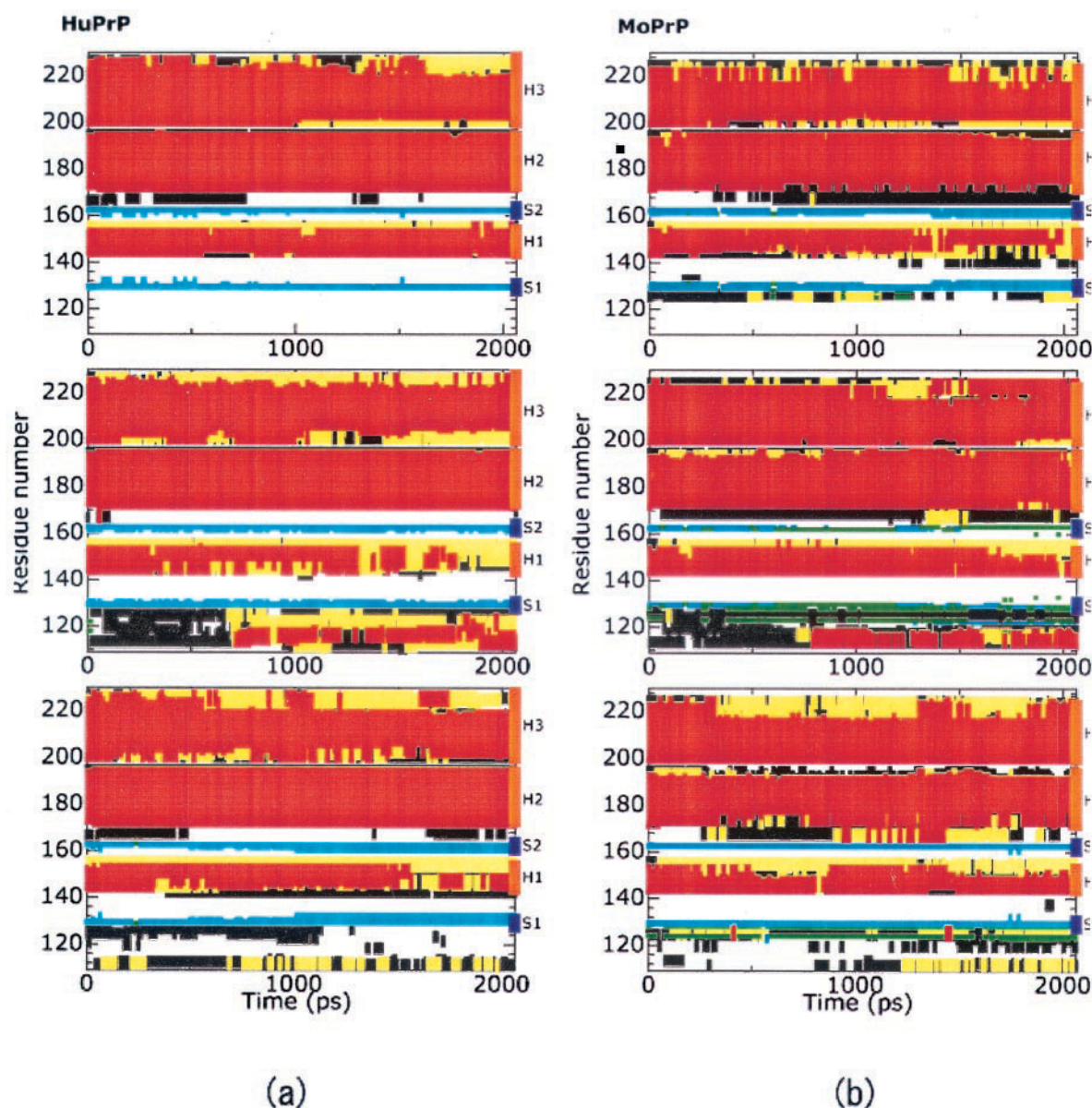
FIGURE 7 Secondary structure as a function of simulation time ((*a*) HuPrP and (*b*) MoPrP). Top figures show control structures, middle figures show wild structures, and bottom figures show mutant structures. The α-helix is shown in a red box, 3_{10}-helix in a yellow box, β-sheet in a blue box, β-bridge in a green box, and turn in a black box.

The average structure (Fig. 6 *b*) showed that H1 was deformed and somewhat unstable. The instability of H1 would be a cause to form the hydrogen bonds of Tyr^{150}-OH–Arg^{136}O and Tyr^{150}OH–Pro^{137}O, which were not observed in the initial structure. Parts other than H1 in the globular domain were similar to those of the initial structure. Analysis of the secondary structure (Fig. 7 *a*) also indicated that H1 changed from an α-helix to a 3_{10}-helix and then become unstable. Thus, the decrease in the α-helix content and the increase in the 3_{10}-helix content in the wild structure were mainly due to a structural change in H1 (Table 2). This mobility of H1 is supported by NMR ex-

periment (García et al., 2000). The H2, H3, and short antiparallel β-sheet in the globular domain were stably maintained for 2 ns in the same manner as the control structure (Fig. 7 *a*). Table 3 shows positions of secondary structure elements. It is obvious from this table that the globular domain of the wild structure was similar to that of the control structure, although a new α-helix (H0), which was not observed in the control and mutant structures, was generated. It was seen in the contact map (Fig. 8 *b*) that H0 was close to H2. Analyses of RMSD and secondary structures indicated that the interaction between H0 and H2 did not influence the structure of the globular domain.
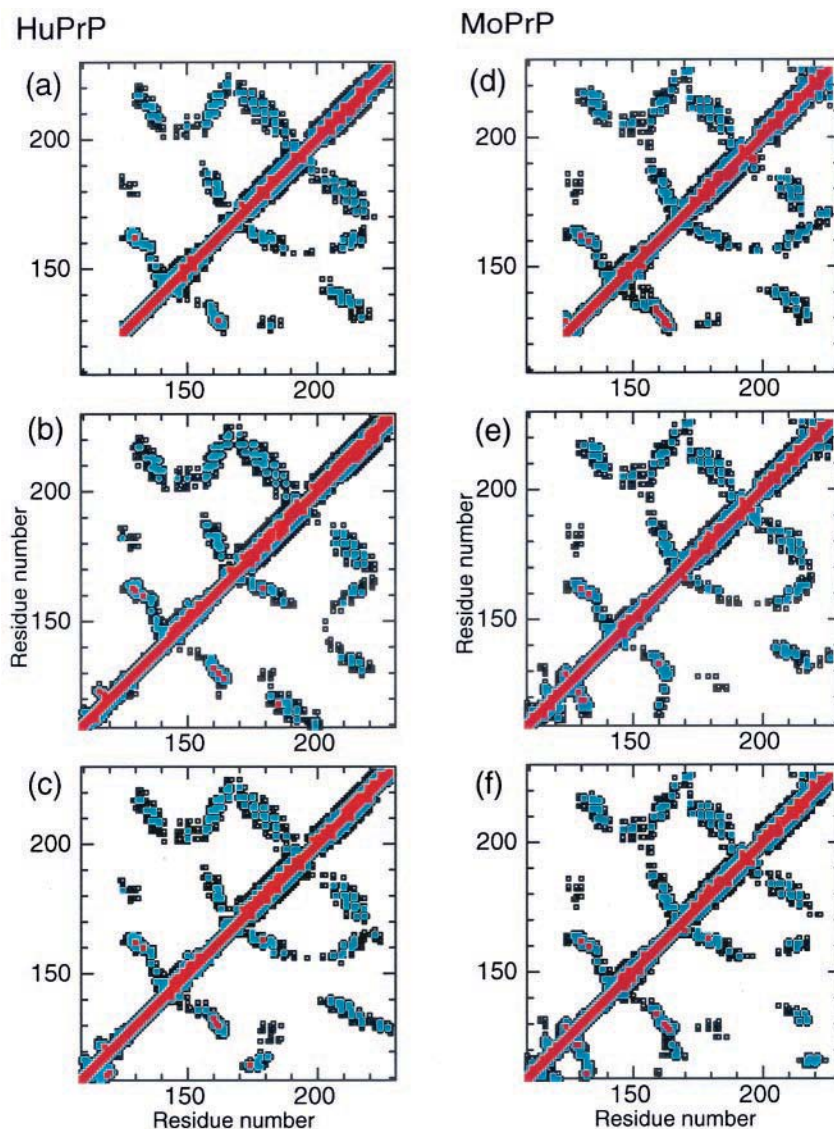
HuPrP

MoPrP

FIGURE 8   Contact map ((*a*) control model of HuPrP; (*b*) wild model of HuPrP; (*c*) mutant model of HuPrP; (*d*) control model of MoPrP; (*e*) wild model of MoPrP; and (*f*) mutant model of MoPrP). Left upper and right lower triangles in each graph indicate the initial and final structures of MD simulation, respectively. The distance within 5 Å is shown in red, the distance 5 to 8 Å in blue, and the distance 8 to 11 Å by open squares.

An interesting finding in the MD simulation of the mutant structure was that the original antiparallel β-sheet had been extended. The average structure (Fig. 6 *c*) clearly indicated the extension of the β-sheet. Analysis of the secondary structures (Fig. 7 *a*; Table 2) indicated that the extension of the β-sheet occurred from 1 ns and that the β-sheet content (8.12 residues) was approximately two-times greater than those of the control and wild structures (3.67 and 4.65 residues, respectively). The H1 region, which is between S1 and S2, was deformed with this extension of the original β-sheet, and, as a consequence, the central part of H1 collapsed (Fig. 6 *c*; Table 3). The collapse of H1 gave rise to the disappearance of even the two hydrogen bonds (Tyr[150]OH–Arg[136]O and Tyr[150]OH–Pro[137]O) that were formed in the MD simulation of the wild structure.

We speculate that the mechanism of the extension of the β-sheet in MD simulation of the mutant structure is as

follows. The main reason for the extension is the behavior of the extra peptide chain in the N-terminal region containing Val[117]. This extra peptide chain does not form a secondary structure, such as an α-helix, due to the effect of Val[117] and it sways flexibly (Figs. 6 *c* and 7 *a*). Its motion induces a structural change in strand 1, which is linked to S1, and then strand 1 approaches strand 2, which is located between H1 and S2. As a result, extension of the β-sheet occurs. In addition, residues 120-127 in the extra peptide chain interacted with the C-terminal side of H3 (Fig. 8 *c*), so that the α-helix of H3 was unlaced and was divided into two parts (Table 3). On the other hand, H2 was not directly affected by the extra peptide chain, and it was stably maintained (Fig. 7 *a*). Thus, the large RMSD values of the globular domain (Fig. 4 *b*) arise from structural changes in strand1, H1, and H3.

TABLE 2 Secondary structure for the final 1-ns MD simulations

	Number of residues	3_{10}-Helix	α-Helix	β-Bridge	β-Sheet	Strand	Turn
Control	104	7.56	55.13	0.05	3.67	1.82	7.98
	(103)	(11.34)	(44.25)	(0.14)	(6.20)	(1.78)	(21.35)
	104*	15.31*	47.14*	0.00*	4.65*	1.86*	10.32*
	(103)*	(8.79)*	(53.75)*	(1.55)*	(1.74)*	(0.79)*	(13.67)*
Wild	120	21.36	50.20	0.00	4.65	1.86	15.19
	(118)	(9.78)	(58.04)	(2.05)	(2.74)	(1.22)	(16.80)
Mutant	104*	12.45*	46.31*	0.01*	8.12*	1.78*	12.18*
	(103)*	(12.79)*	(50.04)*	(1.65)*	(3.94)*	(1.92)*	(11.08)*
	120	13.55	46.31	0.01	8.12	1.78	15.07
	(118)	(14.92)	(50.06)	(1.88)	(3.94)	(1.92)	(15.31)

Numbers are the average numbers of amino acids for the final 1-ns MD simulation.

The data for HuPrP are shown without parentheses, and the data for MoPrP are shown in parentheses.

*Secondary structure content of the globular domain.

TABLE 3 Positions of secondary structure elements for NMR experiments and MD simulation structures of HuPrP and MoPrP models

	NMR experiment	Control	Wild	Mutant
S1	128–131	129–130	129–130	129–133
	(128–133)	(129–132)	(128–129)	(128–130)
S2	161–164	162–163	162–163	160–164
	(161–164)	(160–163)	(162–163)	(162–163)
H1	144–154	145–157	145–157	145–150, 152–157[†]
	(144–153)	(145–157)	(143–157)	(143–157)
H2	173–194	171–195	171–195	171–195
	(172–194)	(175–194)	(172–195)	(172–192)
H3	200–228	200–228	200–228	201–219, 222–228[†]
	(200–224)	(199–223)	(199–226)	(200–226)
S0*	–	–	–	–
	(–)	(–)	(–)	(124)
H0*	–	–	112–124	–
	(–)	(–)	(112–117)	(–)

The data for HuPrP are shown without parentheses, and the data for MoPrP are shown in parentheses. Positions of H0–H3 correspond to residues forming α-helix or 3_{10}-helix and those of S0–S2 correspond to residues forming β-sheet or β-bridge.

*S0 and H0 are additional β-sheet and α-helix in residues 104–124, respectively.

[†]α-Helix is split.

MoPrP

The average structure of the control model (Fig. 9 *a*) shows that the globular domain was stably maintained, although some deformation of the H3 region was seen. A contact map (Fig. 8 *d*) also revealed that the initial and final structures of MD simulation were the same except for some slight differences. The data of secondary structures (Fig. 7 *b*) indicated that H2 was stable, whereas the 3_{10}-helix contents of H1 and H3 increased compared with those of HuPrP, suggesting the instabilities of H1 and H3 that would have arisen due to the difference between the primary structures of HuPrP and MoPrP. In addition, it was noted that the β-sheet content increased from 1.5 ns (Fig. 7 *b*); thereby, its content (6.20 amino acid residues) was more than those of wild and mutant structures of MoPrP and the control and wild structures of HuPrP (Table 2).

In the case of the wild structure, the extra peptide chain (residues 112-117) of the N-terminal region formed a new α-helix (H0) in the same manner as that of HuPrP (Figs. 9 *b* and 7 *b*; Table 3). This extra peptide chain began to form α- and 3_{10}-helices from approximately 800 ps in the MD simulation. In addition, residues 123-124 of the extra peptide chain formed a β-bridge with S1, and synchronously the β-sheet content, which consisted of S1 and S2, decreased. A contact map (Fig. 8 *e*) indicated that residues 123-124 were close to the β-sheet (S1 and S2) but that the approach of these residues to the β-sheet did not affect the conformation of the globular domain.

In MD simulation of the mutant structure, we observed that the relative positions among three α-helices (H1, H2, and H3) of the globular domain were very different from those in the control and wild structures (Fig. 9 *c*). H1, in particular, moved a long distance from its initial position (Fig. 5 *b*), and this movement would have induced the extension of the distances of H1-H3 (Fig. 8 *f*). The analysis of the secondary structure (Fig. 7 *b*) clearly showed that the extra peptide chain formed a β-bridge with S1 in the same manner as that in the wild structure of MoPrP but that was largely unstructured and did not form an α-helix. Moreover, a contact map (Fig. 8 *f*) indicated that the residues 115-117 of the extra peptide chain interacted with the C-terminal side of H3. We speculate that this interaction and the high instability of H1 caused the large RMSD values of the globular domain.

Electric structure

The electronic states of the extra peptide chains (109-124) in the wild and mutant structures were analyzed using semiempirical molecular orbital calculations (modified neglect of diatomic overlap parametric method 3). Fig. 10 shows the isosurface for an electron density of 0.0003 e/Bohr^3 in the high occupied molecular orbital (HOMO). From the lowest unoccupied molecular orbital (LUMO) to the third LUMO, there was no difference between the electronic structures of the wild and mutant models. Notable differences were also not seen between these models from the fourth LUMO to the tenth LUMO (data not shown). On the other hand, we observed a clear difference between the electric structures at the third HOMO, although no differences were seen in the cases of HOMO and the second HOMO (Fig. 10). At the third HOMO, the mutant model only has the electron distribution in peptide chain 119-122,
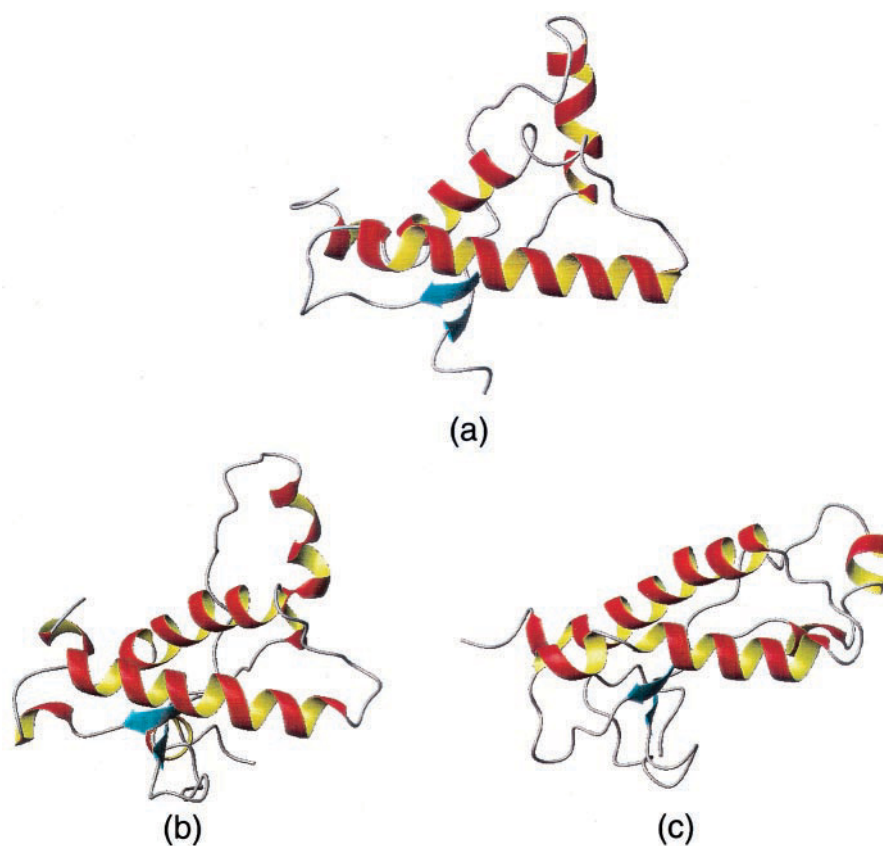
FIGURE 9 Average structures of MoPrP models ((*a*) control structure, (*b*) wild structure, and (*c*) mutant structure). These structures were obtained from the final 1-ns MD simulations.

and it has higher reactivity at residues 119-122 by Ala[117]→Val mutation. We speculate that this high reactivity is a driving force for the motion of the extra peptide chain containing Val[117]. Such high reactivity would be related to the interaction of the extra peptide chain in the N-terminal region with the globular domain in MD simulation of the mutant structure.

DISCUSSION

MD simulations of the control, wild, and mutant structures of HuPrP and MoPrP showed that they have some common features. The most remarkable common feature is that the globular domain of the wild structure was stable and retained the same conformation as that of the control structure, whereas that of mutant structure was unstable. The reason for this is as follows. The extra peptide chain in the wild structure formed an α-helix and was maintained stably, and it therefore did not affect the structure of the globular domain. The extra peptide chain in the mutant structure containing Val[117], however, formed few secondary structures, such as an α-helix and β-sheet, and it could therefore move flexibly to interact with the globular domain.

MD simulation showed that the control structures of HuPrP and MoPrP were similar to the respective NMR structures, although H1 and H3 were somewhat unstable in

MoPrP. Thus, the MD simulations revealed that globular domains, which were determined by experiments of NMR, were stably maintained. MD simulations of the wild structures of HuPrP and MoPrP indicated that the extra peptide chain in the N-terminal region tended to form an α-helix. Gready and co-workers reported the results of MD simulations using HuPrP that was built based on ShPrP (Zuegg and Gready, 1999). Their MD simulations (800 ps) also indicated that α- and 3_{10}-helices were formed in 110-120 residues. Therefore, simulations in our studies and those in their study show similar tendencies. Accordingly, at least theoretical simulations intimated a potential of 110-120 residues to form an α-helix. The experimental data of NMR showed that the N-terminal region except for the globular domain was flexible and had a disordered structure (Riek et al., 1997; Zahn et al., 2000). To examine the reason for the above in compatibility between simulations and experiments, further study should be needed on the conformation of the 109-124 part of wild structure. MD simulations of the mutant structure provided us very important information. The results for HuPrP indicated that the original short antiparallel β-sheet was extended greatly. This phenomenon would be the first step in the mechanism of structural change from PrP[C] to PrP[SC] by Ala[117]→Val mutation. That is, the first step in the PrP[C]→PrP[SC] mechanism is as follows. The structural change in strand 1 between S1 and H1
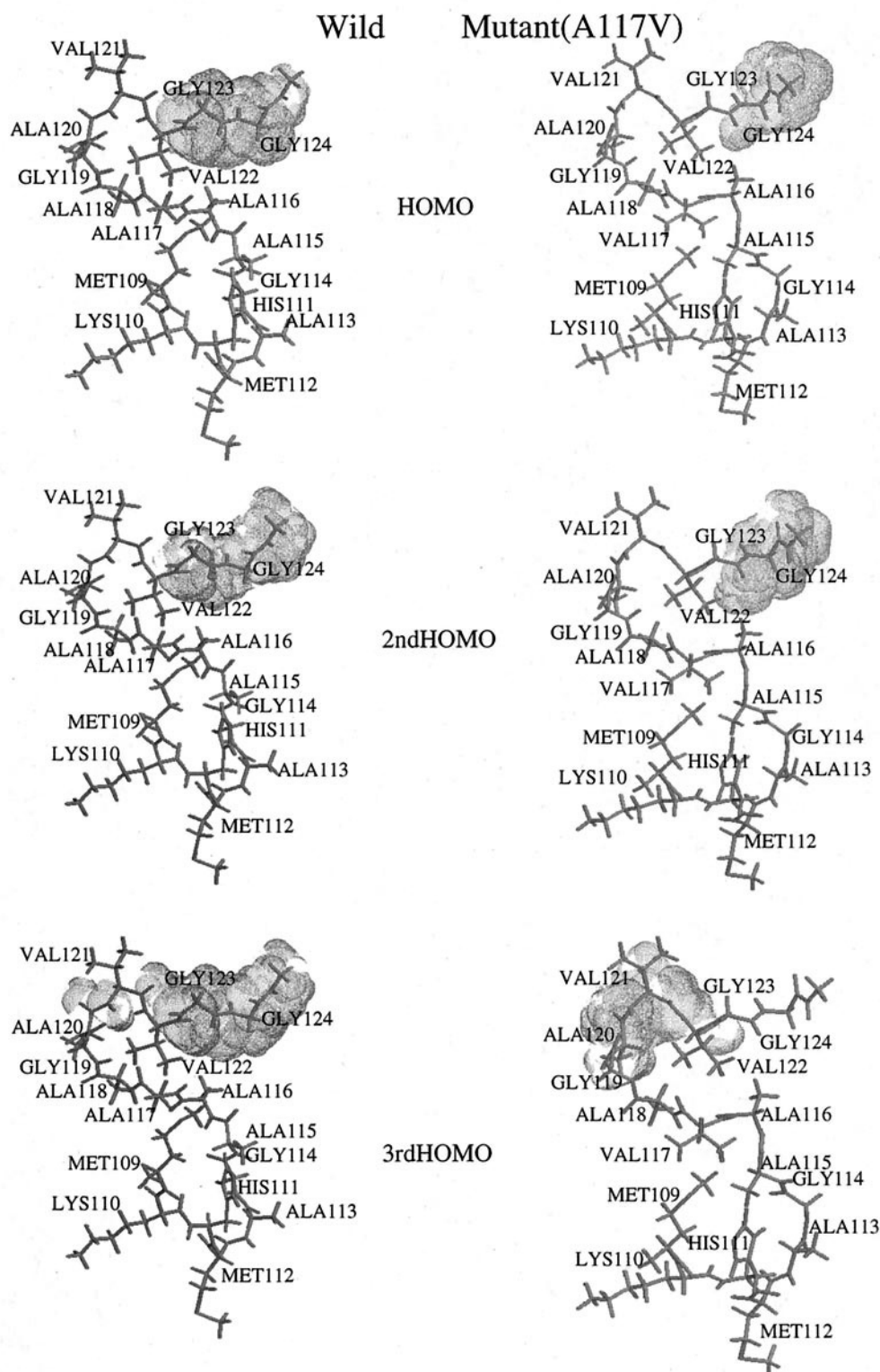
FIGURE 10   Electron distributions in HOMO, second HOMO, and third HOMO. Isosurfaces for electron density of 0.0003 e/Bohr^3 are shown in dots. The figures on the left are wild models, and the figures on the right are mutant models.

occurred due to a flexible motion of the N-terminal region (109-124), and then strand 1 approached strand 2 between H1 and S2. Consequently, the original β-sheet was extended. Accompanying this extension, a deformation of the globular domain, involving collapse of H1, occurred. It is known that H1 is very hydrophilic and that other parts of the globular domain are very hydrophobic, and interaction between them is therefore weak (Morrissey and Shakhnovich, 1999). Experiments performed by Korth et al. (1997) using a monoclonal antibody showed that structures of H1 in PrP^C and PrP^{SC} were different, which is compatible with our result in terms of the deformation of H1 in mutant structure. In addition, experiments performed by Hanan et al. (2001) using a monoclonal antibody showed that the peptide chain 106-126 played an important role in the structural change of PrP^C. These results supported our computational results regarding the dynamic motion of H1 and the peptide chain (109-124). After the above-mentioned structural change, the β-sheet would be extended far more in accordance with the completion of PrP^{SC}. Because an experiment using peptide 106-126 showed that Ala$^{117}\rightarrow$Val mutation increased the β-sheet structure (Brown 2000), it is thought that the extra peptide chain containing Val^{117} is involved in the extension of the β-sheet. A study on point mutations of inherited diseases involving HuPrP revealed that not all mutations reduced the thermal stabilities of the globular domain (Liemann and Glockshuber, 1999). However, the current molecular dynamics study demonstrated that thermal stability of the globular domain is decreased due to the Ala$^{117}\rightarrow$Val mutation.

Although these simulations have not yet perfectly been finished in the whole process of structural change from PrP^C into PrP^{SC}, rapid increase of computational resource, such as molecular dynamics machine (Narumi et al., 2001), will enable us to realize it.

CONCLUSIONS

We provide the following conclusion from this study. Ala$^{117}\rightarrow$Val mutation deforms the structures of the globular domains on HuPrP and MoPrP. Especially in HuPrP containing Val^{117}, the extension of the β-sheet and the collapse of H1 occur. PrP^C containing Ala^{117} tended to form α-helix in the extra peptide chain (109-124 in HuPrP and 109-123 in MoPrP). The extra peptide chain 119-122) containing Val^{117} takes high electron distribution in some frontier molecular orbitals and had a high reactivity. These would be the driving force for the flexible motion of the N-terminal region of the mutant structure.

REFERENCES

Berendsen, H. J. C., J. P. M. Postma, W. F. van Gunsteren, A. DiNola, and J. R. Haak. 1984. Molecular dynamics with coupling to an external bath. *J. Chem. Phys.* 81:3684–3690.

Berman, H. M., J. Westbrook, Z. Feng, G. Gilliland, T. N. Bhat, H. Weissig, I. N. Shindyalov, and P. E. Bourne. 2000. The Protein Data Bank. *Nucleic Acids Res.* 28:235–242.

Borchelt, D. R., M. Scott, A. Taraboulos, N. Stahl, and S. B. Prusiner. 1990. Scrapie and cellular prion proteins differ in their kinetics of synthesis and topology in cultured cells. *J. Cell. Biol.* 110:743–752.

Brown, D. R. 2000. Altered toxicity of the prion protein peptide PrP 106-126 carrying the Ala$^{117}\rightarrow$Val mutation. *Biochem. J.* 346:785–791.

Case, D. A., D. A. Pearlman, J. W. Caldwell, T. E. Cheatham, III, W. S. Ross, C. L. Simmerling, T. A. Darden, K. M. Merz, R. V. Stanton, A. L. Cheng, J. J. Vincent, M. Crowley, D. M. Ferguson, R. J. Radmer, G. L. Seibel, U. C. Singh, P. K. Weiner, and P. A. Kollman. 1997. AMBER 5. University of California, San Francisco, CA.

Cornell, W. D., P. Cieplak, C. I. Bayly, I. R. Gould, K. M. Merz, Jr., D. M. Ferguson, D. C. Spellmeyer, T. Fox, J. W. Caldwell, and P. A. Kollman. 1995. A second generation forth field for the simulation of proteins and nucleic acids. *J. Am. Chem. Soc.* 117:5179–5197.

Donne, D. G., J. H. Viles, D. Groth, I. Mehlhorn, T. L. James, F. E. Cohen, S. B. Prusiner, P. E. Wright, and H. J. Dyson. 1997. Structure of the recombinant full-length hamster prion protein PrP (29-231): the N terminus is highly flexible. *Proc. Natl. Acad. Sci. U. S. A.* 94:13452–13457.

García, L. F., R., Zahn., R., Riek and, K., Wuthrich. 2000. NMR structure of the bovine prion protein. *Proc. Natl. Acad. Sci. U. S. A.* 97:8334–8339.

Hanan, E., O. Goren, M. Eshkenazy, and B. Solomon. 2001. Immunomodulation of the human prion peptide 106-126 aggregation. *Biochem. Biophys. Res. Commun.* 280:115–120.

Hsiao, K., H. F. Baker, T. J. Crow, M. Poulter, F. Owen, J. D. Terwilliger, D. Westaway, J. Ott, and S. B. Prusiner. 1989. Linkage of a prion protein missense variant to Gerstmann-Straussler syndrome. *Nature.* 338:342–345.

Hsiao, K. K., C. Cass, G. D. Schellenberg, T. Bird, E. Devine-Gage, H. Wisniewski, and S. B. Prusiner. 1991. A prion protein variant in a family with the telencephalic form of Gerstmann-Strausser-Scheinker syndrome. *Neurology.* 41:681–684.

James, T. L., H. Liu, N. B. Ulyanov, S. Farr-Jones, H. Zhang, D. G. Donne, K. Kaneko, D. Groth, I. Mehlhorn, S. B. Prusiner, and F. E. Cohen. 1997. Solution structure of a 142-residue recombinant prion protein corresponding to the infectious fragment of the scrapie isoform. *Proc. Natl. Acad. Sci. U. S. A.* 94:10086–10091.

Jorgensen, W. L., J. Chandrasekhar, and J. D. Madura. 1983. Comparison of simple potential functions for simulating liquid water. *J. Chem. Phys.* 79:926–935.

Koradi, R., M. Billeter, and K. Wuthrich. 1996. MOLMOL: a program for display and analysis of macromolecular structure. *J. Mol. Graphics.* 4:51–55.

Korth, C., B. Stierli, P. Streit, M. Moser, O. Schaller, R. Fischer, W. Schulz-Schaeffer, H. Kretzschmar, A. Raeber, U. Braun, F. Ehrensperger, S. Hornemann, R. Glockshuber R. Riek, M. Billeter, K. Wuthrich, and B. Oesch. 1997. Prion (PrP ^{sc})-specific epitope defined by a monoclonal antibody. *Nature.* 390:74–77.

Kretzschmar, H. A. 1993. Human prion diseases (spongiform encephalopathies). *Arch. Virl. Suppl.* 7:261–293.

Laskowski, R. A., M. W. MacArthur, D. S. Moss, and J. M. Thornton. 1993. PROCHECK: a program to check the stereochemical quality of protein structures. *J. Appl. Cryst.* 26:283–291.

Liemann, S., and R. Glockshuber, R. 1999. Influence of amino acid substitutions related to inherited human prion diseases on the thermodynamic stability of the cellular prion protein. *Biochemistry.* 38:3258–3267.

Liu, H., S. Farr-Jones, N. B. Ulyanov, M. Llinas, S. Marqusee, D. Groth, F. E. Cohen, S. B. Prusiner, and T. L. James. 1999. Solution structure of

Syrian hamster prion protein rPrP (29–231). *Biochemistry.* 38: 5362–5377.

Mastrianni, J. A., M. T. Curtis, J. C. Oberholtzer, M. M. Da Costa, S. DeArmond, S. B. Prusiner, and J. Y. Garbern. 1995. Prion disease (PrP -Ala[117]→Val) presenting with ataxia instead of dementia. *Neurology.* 45:2042–2050.

Morrissey, M. P., and E. I. Shakhnovich. 1999. Evidence for the role of PrP[c] helix 1 in the hydrophilic seeding of prion aggregates. *Proc. Natl. Acad. Sci. U. S. A.* 96:11293–11298.

Narumi, T., A. Kawai, and T. Koishi. 2001. An 8.61 Tflop/s Molecular Dynamics Simulation for NaCl with a Special-Purpose Computer: MDM. *In* Proc. SC2001 (CDROM). Assoc. Comp. Machinery, New York.

Pan, K. M., M. Baldwin, J. Nguyen, M. Gasset, A. Serban, D. Groth, I. Mehlehorn, Z. Huang, R. J. Fletterick, F. E. Cohen, and S. B. Prusiner. 1993. Conversion of alpha-helices into beta-sheets features in the formation of the scrapie prion proteins. *Proc. Natl. Acad. Sci. U. S. A.* 90:10962–10966.

Prusiner, S. B., and S. DeArmond. 1994. Biology and genetics of prion diseases. *Annu. Rev. Neurosci.* 17:311–319.

Riek, R., S. Hornemann, G. Wider, M. Billeter, R. Glockshuber, and K. Wuthrich. 1996. NMR structure of the mouse prion protein domain PrP (121–231). *Nature.* 382:180–182.

Riek, R., S. Hornemann, G. Wider, R. Glockshuber, and K. Wuthrich. 1997. NMR characterization of the full-length recombinant murine prion protein, mPrP (23-231). *FEBS Lett.* 413:282–288.

Riek, R., G. Wider, M. Billeter, S. Hornemann, R. Glockshuber, and K. Wuthrich. 1998. Prion protein NMR structure and familial human spongiform encephalopathies. *Proc. Natl. Acad. Sci. U. S. A.* 95: 11667–11672.

Ryckaert, J. P., G. Ciccotti, and H. J. C. Berendsen. 1977. Numerical integration of the Cartesian equations of proteins and nucleic acids. *J. Comput. Phys.* 23:327–341.

Safar, J., P. P. Roller, D. C. Gajdusek, and C. J. Gibbs. 1993. Thermal stability and conformational transitions of scrapie amyloid (prion) protein correlate with infectivity. *Protein Sci.* 2:2206–2216.

Stahl, N., M. A. Baldwin, R. Hecker, K. M. Pan, A. L. Burlingame, and S. B. Prusiner. 1992. Glycosylinositol phospholipid anchors of the scrapie and cellular prion proteins contain sialic acid. *Biochemistry.* 31:5043–5053.

Stahl, N., M. A. Baldwin, D. B. Teplow, L. Hood, B. W. Gibson, A. L. Burlingame, and S. B. Prusiner. 1993. Structural studies of the scrapie prion protein using mass. *Biochemistry.* 32:1991–2002.

Stahl, N., D. R. Borchelt, K. Hsiao, and S. B. Prusiner. 1987. Scrapie prion protein contains a phosphatidylinositol glycolipid. *Cell.* 51:229–240.

Stewart, J. J. P. 1989a. Optimization of parameters for semi-empirical methods I—methods. *J. Comp. Chem.* 10:209–220.

Stewart, J. J. P. 1989b. Optimization of parameters for semi-empirical methods II—applications. *J. Comp. Chem.* 10:221–264.

Stewart, J. J. P., and J. Frank. 1990. Mopac Manual, sixth edition: A General Molecular Orbital Package. Frank J. Seiler Research Laboratory, U.S. Air Force Academy, Colorado Springs, CO.

Tateishi, J., T. Kitamoto, K. Dohura, Y. Sakaki, G. Steinmets, C. Tranchant, J. M. Warter, and N. Heldt. 1990. Immunochemical, molecular genetic, and transmission studies on a case of Gerstmann-Straussler-Sheinker syndrome. *Neurology.* 40:1578–1581.

Telling, G. C., M. Scott, J. Mastrianni, R. Gabizon, M. Torchia, F. E. Cohen, S. J. DeArmond, N. Stahl, and S. B. Prusiner. 1995. Prion propagation in mice expressing human and chimeric PrP transgenes implicates the interaction of cellular PrP with another protein. *Cell.* 83:79–99.

Tranchant, C., N. Sergeant, A. Wattez, M. Mohr, J. M. Warter, and A. Delacourte. 1997. Neurofibrillary tangles in Gerstmann-Straussler-Scheinker syndrome with the Ala[117]→Val prion gene mutation. *J. Neurol. Neurosurg. Psych.* 63:240–246.

Zahn, R., A. Liu, T. Luhrs, R. Riek, C. V. Schroetter, F. L. García, M. Billeter, L. Calzolai, G. Wide, and K. Wuthrich. 2000. NMR solution structure of the human prion protein. *Proc. Natl. Acad. Sci. U. S. A.* 97:145–150.

Zuegg, J., and J. E. Gready. 1999. Molecular dynamics simulations of human prion protein: importance of correct treatment of electrostatic interaction. *Biochemistry.* 38:13862–13876.